



## Enhanced Stability of LiCoO<sub>2</sub> Cathodes in Lithium-Ion Batteries Using Surface Modification by Atomic Layer Deposition

Yoon Seok Jung,<sup>a,\*</sup> Andrew S. Cavanagh,<sup>b</sup> Anne C. Dillon,<sup>c,\*</sup>  
Markus D. Groner,<sup>d</sup> Steven M. George,<sup>e</sup> and Se-Hee Lee<sup>a,\*</sup>

<sup>a</sup>Department of Mechanical Engineering, University of Colorado at Boulder, Boulder, Colorado 80309-0427, USA

<sup>b</sup>Department of Physics, <sup>c</sup>Department of Chemistry and Biochemistry, and Department of Chemical and Biological Engineering, University of Colorado at Boulder, Boulder, Colorado 80309-0215, USA

<sup>e</sup>National Renewable Energy Laboratory, Golden, Colorado 80401, USA

<sup>d</sup>ALD NanoSolutions Incorporated, Broomfield, Colorado 80020, USA

Ultrathin atomic layer deposition (ALD) coatings enhance the performance of lithium-ion batteries (LIBs). Previous studies have demonstrated that LiCoO<sub>2</sub> cathode powders coated with metal oxides with thicknesses of ~100 to 1000 Å grown using wet chemical techniques improved LIB performance. In this study, LiCoO<sub>2</sub> powders were coated with conformal Al<sub>2</sub>O<sub>3</sub> ALD films with thicknesses of only ~3 to 4 Å established using two ALD cycles. The coated LiCoO<sub>2</sub> powders exhibited a capacity retention of 89% after 120 charge–discharge cycles in the 3.3–4.5 V (vs Li/Li<sup>+</sup>) range. In contrast, the bare LiCoO<sub>2</sub> powders displayed only a 45% capacity retention. Al<sub>2</sub>O<sub>3</sub> ALD films coated directly on the composite electrode also produced improved capacity retention. This dramatic improvement may result from the ultrathin Al<sub>2</sub>O<sub>3</sub> ALD film acting to minimize Co dissolution or reduce surface electrolyte reactions. Similar experiments with ultrathin ZnO ALD films did not display enhanced performance.  
© 2009 The Electrochemical Society. [DOI: 10.1149/1.3258274] All rights reserved.

Manuscript submitted July 1, 2009; revised manuscript received October 5, 2009. Published November 18, 2009.

Efficient and durable electrical energy storage is one of the major factors limiting the widespread adoption of renewable energy. Since lithium-ion batteries (LIBs) were first commercialized in the early 1990s, LIBs have emerged as an important energy storage device for portable electronics.<sup>1–3</sup> LIBs are very desirable because of their high energy storage per volume and per mass. However, LIBs with higher stability are needed for their use in plug-in hybrids or all-electric vehicles.

Li<sub>1–x</sub>CoO<sub>2</sub> is the most commercialized cathode material. Unfortunately, the practical use of Li<sub>1–x</sub>CoO<sub>2</sub> is limited because the stability rapidly deteriorates at potentials higher than 4.2–4.3 V (vs Li/Li<sup>+</sup>).<sup>4</sup> Cobalt dissolution, structural changes, and oxidative decomposition of the electrolyte produce a dramatic increase in the capacity fade at the higher potentials.<sup>4</sup> These instabilities can be addressed by coating the LiCoO<sub>2</sub> powders with metal oxide coatings with thicknesses of ~100 to 1000 Å.<sup>5,6</sup> Examples of the metal oxides that have been explored include Al<sub>2</sub>O<sub>3</sub>, ZrO<sub>2</sub>, ZnO, SiO<sub>2</sub>, and TiO<sub>2</sub>.<sup>5,6</sup> Metal phosphates<sup>7</sup> (e.g., AlPO<sub>4</sub>) and metal fluorides<sup>8</sup> (e.g., AlF<sub>3</sub>) have also been studied as coatings.

The majority of the coating strategies have been based on solution techniques such as the sol–gel method.<sup>5–9</sup> These wet chemical coating methods require large amounts of solvent and precursor. A post-heat-treatment is also necessary after the sol–gel coating.<sup>5–9</sup> In contrast, atomic layer deposition (ALD) is a gas-phase method of thin-film growth using sequential, self-limiting surface reactions.<sup>10,11</sup> ALD requires only a minimal amount of precursor, and ALD coatings are conformal and offer atomic thickness control. ALD could be a promising alternative method to coat electrode materials for LIBs. Although ALD films have been employed in a variety of application areas,<sup>12–16</sup> the use of ALD films for LIB electrodes has not been pursued extensively.<sup>17</sup>

In this paper, the electrochemical performance is reported for LiCoO<sub>2</sub> coated with ultrathin conformal Al<sub>2</sub>O<sub>3</sub> and ZnO films by ALD. The experiments examine the effects of the coating material and the coating thickness on cycle performance and rate capability. The viability of ALD is also explored directly on composite elec-

trodes. The results reveal that ultrathin Al<sub>2</sub>O<sub>3</sub> ALD films can dramatically enhance the stability of LiCoO<sub>2</sub> cathodes.

### Experimental

**ALD on LiCoO<sub>2</sub> powders.**— Al<sub>2</sub>O<sub>3</sub> ALD films were grown directly on the LiCoO<sub>2</sub> powders. The precursors utilized for Al<sub>2</sub>O<sub>3</sub> ALD were trimethylaluminum (TMA) and H<sub>2</sub>O, as shown in Fig. 1. The two self-limiting surface reactions that define Al<sub>2</sub>O<sub>3</sub> ALD growth are<sup>18–20</sup>



Al<sub>2</sub>O<sub>3</sub> ALD films are amorphous and pinhole-free with a density of ~3.0 g cm<sup>-3</sup>.<sup>19,21</sup> The typical growth rate for Al<sub>2</sub>O<sub>3</sub> ALD is 1.1–1.2 Å per ALD cycle.<sup>19,20</sup> However, purging H<sub>2</sub>O may be difficult for ALD on high surface area powders. The presence of H<sub>2</sub>O during the TMA reaction may lead to a slightly larger growth per cycle resulting from some chemical vapor deposition.<sup>22,23</sup>

To compare Al<sub>2</sub>O<sub>3</sub> ALD with other ALD materials, ZnO ALD was also grown on LiCoO<sub>2</sub> powders. The ZnO ALD surface chemistry employs Zn(CH<sub>2</sub>CH<sub>3</sub>)<sub>2</sub> (diethylzinc, DEZ) and H<sub>2</sub>O as the reactants. In similarity with Al<sub>2</sub>O<sub>3</sub> ALD, the two self-limiting reaction sequences are<sup>24,25</sup>



The typical growth rate for ZnO ALD is 2.0 Å per ALD cycle.<sup>26</sup> ZnO ALD may also display larger growth rates on powders because of incomplete purging of H<sub>2</sub>O.

ALD on LiCoO<sub>2</sub> powders was performed using a rotary ALD reactor.<sup>22</sup> A schematic of the rotary reactor is shown in Fig. 2. To perform ALD on powders, the powders were placed in a porous stainless steel cylinder (A) in the reaction chamber. The cylinder was positioned on a magnetically coupled shaft via a load lock door (B). A rotor turned the cylinder to agitate the powder (C). A capacitance manometer (D) was used to measure the pressure in the reaction chamber. The introduction of precursor and purge gases was controlled via a series of pneumatic (E) and needle valves (F). To evacuate the chamber, a gate valve (G) was opened to connect the chamber to a vacuum pump (H).

\* Electrochemical Society Active Member.

<sup>c</sup> Present address

<sup>z</sup> E-mail: sehee.lee@colorado.edu

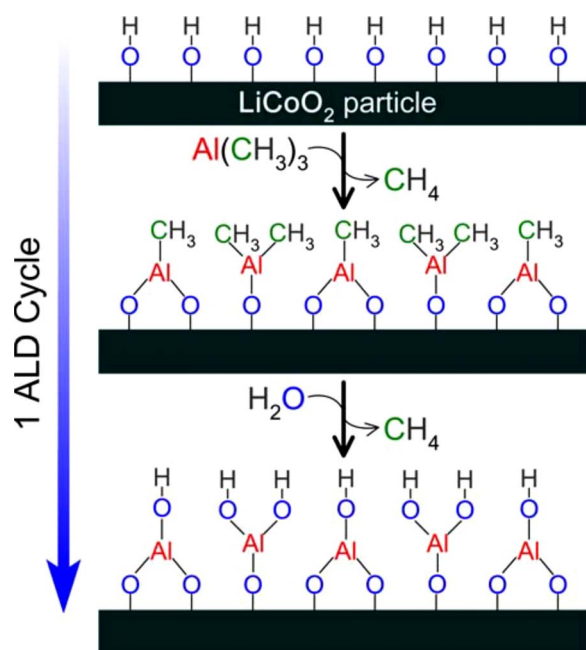


**Figure 1.** (Color online) Schematic representation of  $\text{Al}_2\text{O}_3$  ALD on  $\text{LiCoO}_2$  powders.

The  $\text{Al}_2\text{O}_3$  ( $\text{ZnO}$ ) ALD reaction sequence was: (i) TMA (DEZ) dose to 1.0 (1.0) Torr, (ii) TMA (DEZ) reaction time, (iii) evacuation of the reaction products and excess TMA (DEZ), (iv)  $\text{N}_2$  dose to 20.0 Torr, (v)  $\text{N}_2$  static time, (vi) evacuation of  $\text{N}_2$  and any entrained gases, (vii)  $\text{H}_2\text{O}$  dose to 1.0 Torr, (viii)  $\text{H}_2\text{O}$  reaction time, (ix) evacuation of reaction products and excess  $\text{H}_2\text{O}$ , (x) dose  $\text{N}_2$ , (xi)  $\text{N}_2$  static time, and (xii) evacuation of  $\text{N}_2$  and any entrained gases. This sequence constitutes one cycle of  $\text{Al}_2\text{O}_3$  ( $\text{ZnO}$ ) ALD. Both  $\text{Al}_2\text{O}_3$  ALD and  $\text{ZnO}$  ALD were conducted at  $180^\circ\text{C}$ .

**Material characterization.**—X-ray photoelectron spectroscopy (XPS) measurements were performed on a PHI 5600 X-ray photoelectron spectrometer using a monochromatic  $\text{Al K}\alpha$  source (1486.6 eV). The base pressure in the spectrometer during analysis

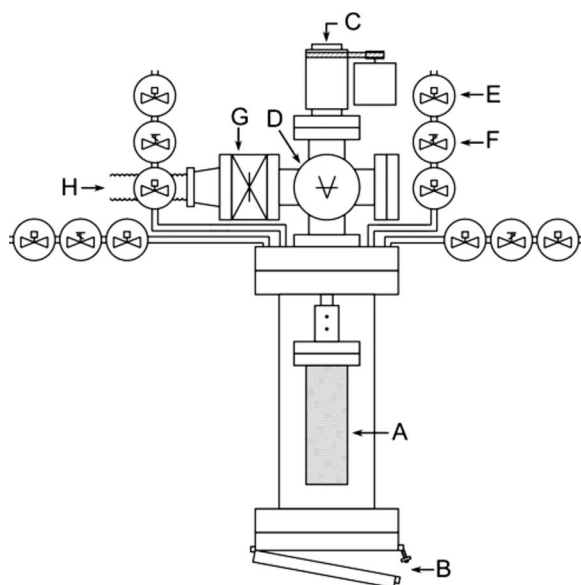


**Figure 2.** Schematic diagram of the rotary ALD reactor.

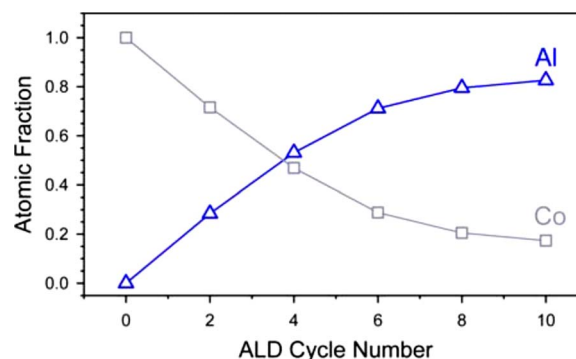


**Figure 3.** (Color online) Atomic fraction of Al and Co for  $\text{Al}_2\text{O}_3$  ALD-coated  $\text{LiCoO}_2$  powders vs the number of ALD cycles. Atomic fraction was determined from XPS spectra.

was  $3 \times 10^{-10}$  Torr. During the data acquisition, the constant analyzer energy mode was employed at pass energies between 58.7 and 93.9 eV and a step size between 0.25 and 0.4 eV. Using the Al 2s and the Co  $2p_{3/2}$  peaks, the growth rate for the  $\text{Al}_2\text{O}_3$  ALD on  $\text{LiCoO}_2$  was determined from thicknesses calculated using a model for flat surfaces.<sup>27,28</sup>

A  $\text{LiCoO}_2$ -embedded Ag foil for obtaining XPS spectra was prepared by pressing ( $\sim 1.5$  GPa) the  $\text{LiCoO}_2$  powders that were spread on a piece of Ag foil with a thickness of 0.5 mm. The composite electrodes were used for the ex situ XPS analysis. Cells were disassembled, and electrodes were rinsed with dimethyl carbonate (DMC) and dried in an Ar-filled dry box. The conductivity of  $\text{LiCoO}_2$  powders was measured by the van der Pauw method<sup>29</sup> using 120 MPa.

**Electrochemical characterization.**—For the galvanostatic charge–discharge cycling, a composite electrode was prepared by spreading a slurry mixture of  $\text{LiCoO}_2$  powder (7–10  $\mu\text{m}$ , L106, LICO Technology), acetylene black (AB), and poly(vinylidene fluoride) (PVDF) (83.0:7.5:9.5 weight ratio) on a piece of Al foil. The cells were assembled in an Ar-filled dry box and tested in a temperature-controlled oven. The galvanostatic charge–discharge cycling was performed with a two-electrode 2032-type coin cell in the potential range of 3.3–4.5 V (vs  $\text{Li/Li}^+$ ) at a current density of 0.1 C rate (14  $\text{mA g}^{-1}$ ) for the first two cycles and 1 C rate for the subsequent cycles at room temperature. Li metal foil was used as the counter electrode.

1.0 M  $\text{LiPF}_6$  dissolved in a mixture of ethylene carbonate, and DMC (1:1 v/v) was used as the electrolyte. A porous 20  $\mu\text{m}$  thick polypropylene (PP)/polyethylene/PP trilayer film was used as the separator. The electrochemical impedance spectroscopy (EIS) study was performed using a 1280C Solartron instrument. The ac impedance measurement was recorded using a signal with an amplitude of 5 mV and a frequency range from 20 kHz to 5 mHz. After the  $\text{LiCoO}_2/\text{Li}$  cells were charged to 4.5 V (vs  $\text{Li/Li}^+$ ) with a current density of 0.1 C rate (14  $\text{mA g}^{-1}$ ) and stabilized by resting for 6 h, the ac impedance spectra were recorded at the open-circuit voltage.

## Results and Discussion

**$\text{Al}_2\text{O}_3$  ALD on  $\text{LiCoO}_2$  powders.**—Figure 3 shows the Al and Co atomic fraction on the  $\text{LiCoO}_2$  powders as determined by XPS vs the number of  $\text{Al}_2\text{O}_3$  ALD cycles. The rapid attenuation of the Al signal is evidence that the  $\text{Al}_2\text{O}_3$  ALD is conformally coating the  $\text{LiCoO}_2$  powders. The conformality of  $\text{Al}_2\text{O}_3$  ALD films on particles has also been verified with transmission electron microscopy.<sup>23</sup> If the attenuation of the Co signal is modeled as  $\text{Al}_2\text{O}_3$  grown on a flat  $\text{LiCoO}_2$  surface,<sup>27</sup> XPS analysis indicates a growth rate of 2.2 Å per

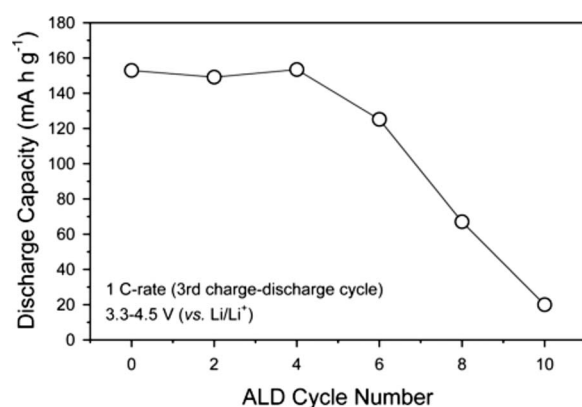


**Figure 4.** Specific discharge capacity of  $\text{Al}_2\text{O}_3$  ALD-coated  $\text{LiCoO}_2$  electrodes vs the number of ALD cycles.

ALD cycle. A higher  $\text{Al}_2\text{O}_3$  ALD growth rate than expected is attributed to the incomplete purging of  $\text{H}_2\text{O}$  from the  $\text{LiCoO}_2$  powders during  $\text{Al}_2\text{O}_3$  ALD.<sup>22,23</sup>

Figure 4 plots the specific discharge capacity for a current density of 1 C rate ( $140 \text{ mA g}^{-1}$ ) during the third charge–discharge cycle vs the number of  $\text{Al}_2\text{O}_3$  ALD cycles deposited on the  $\text{LiCoO}_2$  powders. The capacity during the third charge–discharge cycle does not change considerably for up to four ALD cycles. After six ALD cycles, the capacity starts to decrease significantly and shows a negligible value of  $\sim 20 \text{ mAh g}^{-1}$  after the 10th ALD cycle. The loss of capacity is attributed to the large overpotential required for the  $\text{LiCoO}_2$  powders coated with more than six ALD cycles. These large overpotentials for  $>6$  ALD cycles are shown in Fig. 5.

The loss of capacity results mainly from the electronically insulating character of the  $\text{Al}_2\text{O}_3$  ALD film.<sup>21</sup> The conductivities measured using the van der Pauw method are shown in Fig. 6. The bare  $\text{LiCoO}_2$  powders have an electronic conductivity of  $2 \times 10^{-4} \text{ S cm}^{-1}$ . After only two ALD cycles, the electronic conductivity is significantly reduced to  $5 \times 10^{-5} \text{ S cm}^{-1}$ . The conductivity continuously decreases with increasing number of ALD cycles.

An  $\text{Al}_2\text{O}_3$  ALD film with a thickness of  $>10 \text{ Å}$  after six ALD cycles on the  $\text{LiCoO}_2$  powders significantly reduces the electronic conductivity. The reduction in electron conductivity could result in

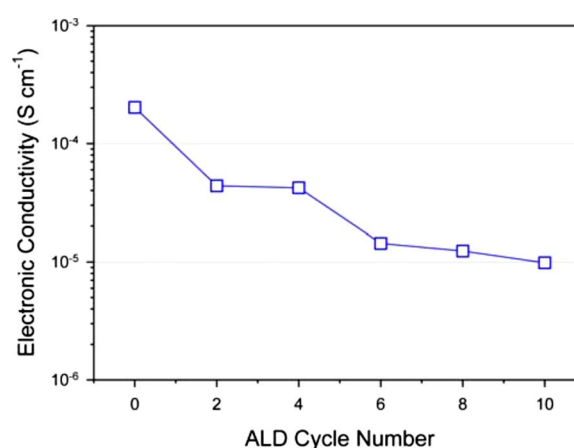


**Figure 6.** (Color online) Electronic conductivity of bare and  $\text{Al}_2\text{O}_3$  ALD-coated  $\text{LiCoO}_2$  powders.

slower charge/discharge kinetics. The  $\text{Al}_2\text{O}_3$  ALD film could also reduce lithium-ion conductivity. However, some previous studies have reported faster Li diffusion in the  $\text{Al}_2\text{O}_3$ -coated  $\text{LiCoO}_2$  resulting from a thin  $\text{LiCo}_{1-x}\text{Al}_x\text{O}_2$  solid solution layer.<sup>30,31</sup> Likewise, other investigations report increases in electrical conductivity for  $\text{Al}_2\text{O}_3$ -coated  $\text{LiCoO}_2$ .<sup>32</sup> These reports of a faster Li diffusion and a higher electrical conductivity for  $\text{Al}_2\text{O}_3$ -coated  $\text{LiCoO}_2$  are surprising given that the  $\text{LiCoO}_2$  powders have been coated by films with thicknesses of  $\sim 100$  to  $1000 \text{ Å}$  using wet chemical methods.

The final step is a post-heat-treatment for many of the wet chemical methods. This heat-treatment may lead to interdiffusion between the  $\text{Al}_2\text{O}_3$  layer and the  $\text{LiCoO}_2$  core, resulting in an amorphous  $\text{LiAl}_x\text{Co}_{1-x}\text{O}_2$  solid solution.<sup>9,33</sup> This  $\text{LiAl}_x\text{Co}_{1-x}\text{O}_2$  alloy may be responsible for the enhanced  $\text{Li}^+$ -ion transport properties and increased electronic conductivity. To examine the effect of the heat-treatment,  $\text{LiCoO}_2$  powders coated with 20 cycles of  $\text{Al}_2\text{O}_3$  ALD were heat-treated at  $450^\circ\text{C}$  for 10 h in air. The discharge capacity before the heat-treatment was  $\sim 8 \text{ mAh g}^{-1}$  at 1 C rate. After the heat-treatment, the discharge capacity was slightly increased to  $15 \text{ mAh g}^{-1}$ , as shown in Fig. 7. Because the heat-treatment did not significantly enhance the discharge capacity to values

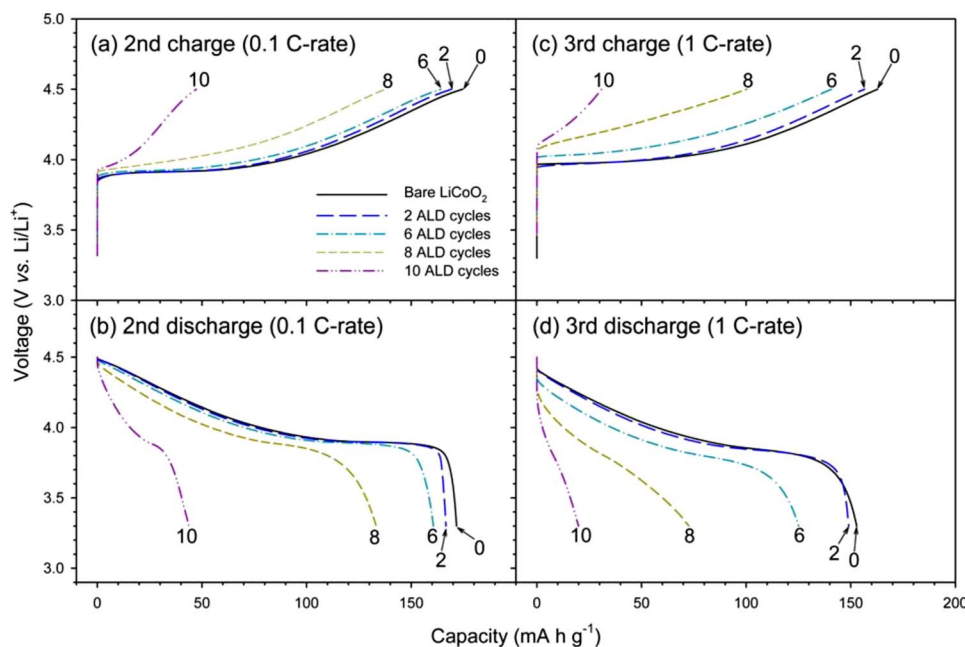


**Figure 5.** (Color online) The second and third charge–discharge voltage profiles of electrodes fabricated using bare and  $\text{Al}_2\text{O}_3$  ALD-coated  $\text{LiCoO}_2$  powders. The ALD was performed on the bare  $\text{LiCoO}_2$  powders. The current densities for the second and third charge–discharge cycles were 0.1 and 1 C rate, respectively.

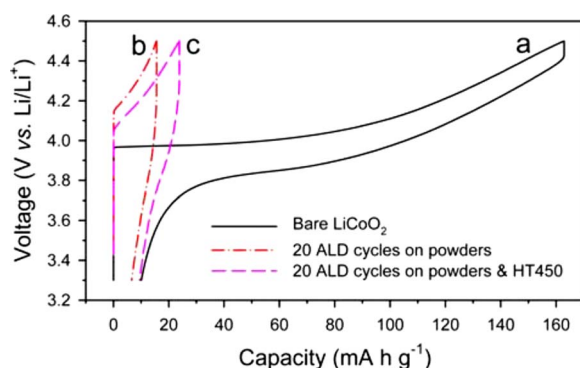


**Figure 7.** (Color online) Charge-discharge voltage profiles at the third charge-discharge cycle (1 C rate). (a) Electrode prepared from the bare  $\text{LiCoO}_2$  powder. Electrodes prepared using  $\text{LiCoO}_2$  powders after (b) 20  $\text{Al}_2\text{O}_3$  ALD cycles and (c) 20  $\text{Al}_2\text{O}_3$  ALD cycles and subsequent heat-treatment at  $450^\circ\text{C}$  for 10 h in air.

$>100 \text{ mAh g}^{-1}$ , the effect of the ALD coatings is attributed to the high quality conformal insulation provided by the  $\text{Al}_2\text{O}_3$  ALD coating compared with previous  $\text{Al}_2\text{O}_3$  films grown using wet chemical techniques.

Figure 8 compares the cycle performance for several electrodes when cycled in the range of 3.3–4.5 V (vs  $\text{Li/Li}^+$ ) with a current density of 0.1 C rate ( $14 \text{ mA g}^{-1}$ ) for the first two cycles and 1 C rate for the subsequent cycles. The initial capacity of  $\text{LiCoO}_2$  powders coated with  $\text{Al}_2\text{O}_3$  ALD using two ALD cycles is similar to the initial capacity of bare  $\text{LiCoO}_2$  powders. Based on the XPS results, the thicknesses of the  $\text{Al}_2\text{O}_3$  ALD film after two ALD cycles are  $\sim 3$  to  $4 \text{ \AA}$ . The initial capacity decreases for 6 and 10 ALD cycles as the current density increases from 0.1 to 1 C rate. This reduction in capacity is attributed to the restricted electron transport and possibly to the slower  $\text{Li}^+$  diffusion kinetics in the  $\text{Al}_2\text{O}_3$  ALD layer.

The  $\text{LiCoO}_2$  powders coated with  $\text{Al}_2\text{O}_3$  ALD show a dramatically improved retention of capacity vs the charge/discharge cycle number regardless of the ALD coating thickness. The coated  $\text{LiCoO}_2$  powders exhibited a capacity retention of 89% after 120 charge-discharge cycles in the 3.3–4.5 V (vs  $\text{Li/Li}^+$ ) range. In contrast, the bare  $\text{LiCoO}_2$  powders displayed only a 45% capacity retention. The stability is highest after 10 ALD cycles although these electrodes have severely restricted capacity because of the insulating  $\text{Al}_2\text{O}_3$  ALD layer.

Figure 9 shows the charge-discharge voltage profiles for the electrodes fabricated with bare  $\text{LiCoO}_2$  powders and  $\text{Al}_2\text{O}_3$  ALD-

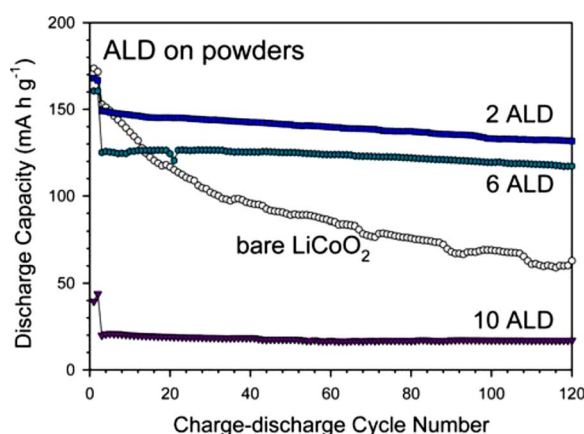


**Figure 8.** (Color online) Charge-discharge cycle performance of electrodes fabricated using the bare  $\text{LiCoO}_2$  powders and the  $\text{Al}_2\text{O}_3$  ALD-coated  $\text{LiCoO}_2$  powders using 2, 6, and 10 ALD cycles.

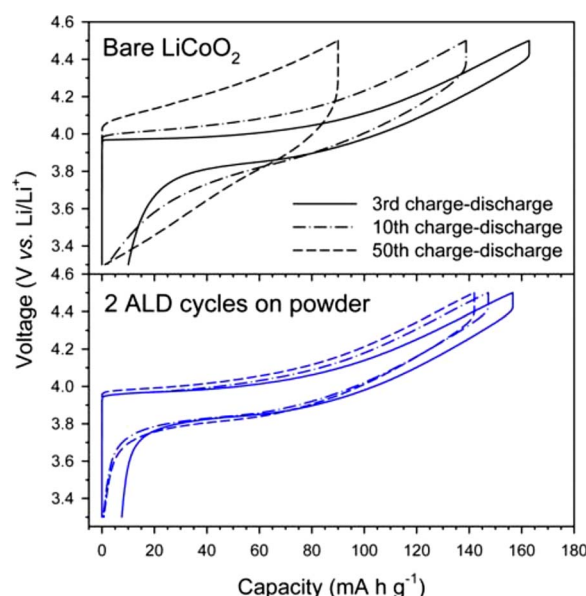


**Figure 9.** (Color online) Charge-discharge voltage profiles of electrodes fabricated with the bare and the  $\text{Al}_2\text{O}_3$  ALD-coated  $\text{LiCoO}_2$  powders at the 3rd, 10th, and 50th cycles when cycled at a current density of 1 C rate ( $140 \text{ mA g}^{-1}$ ).

coated  $\text{LiCoO}_2$  powders using two ALD cycles. The voltage profiles reveal the changing behavior of the bare  $\text{LiCoO}_2$  powders. The polarization increases and the specific capacity drops rapidly vs the charge/discharge cycle number for the electrodes prepared using the bare  $\text{LiCoO}_2$  powders. In contrast, the voltage profile and specific capacity do not change significantly for the electrodes fabricated using the  $\text{Al}_2\text{O}_3$  ALD-coated  $\text{LiCoO}_2$  powders.

EIS analyses were also utilized to evaluate the performance of the electrodes prepared using bare  $\text{LiCoO}_2$  powders and  $\text{Al}_2\text{O}_3$  ALD-coated  $\text{LiCoO}_2$  powders prepared using two ALD cycles. Results showing the Nyquist plots vs the number of charge-discharge cycles are shown in Fig. 10.  $Z'$  ( $\Omega \text{ g}$ ) is the magnitude of the real impedance and  $-Z''$  ( $\Omega \text{ g}$ ) is the magnitude of the imaginary impedance.

The impedance spectra for bare  $\text{LiCoO}_2$  powders follow the typical spectra of  $\text{LiCoO}_2$ , which comprise two semicircles and a  $45^\circ$  inclined line.<sup>34,35</sup> The first semicircle in the higher frequency zone (#) is related to the solid electrolyte interphase, while the second semicircle in the lower frequency zone (\*) is a charge-transfer reaction at the electrolyte/electrode interface.<sup>34,35</sup> The charge-transfer resistance at the  $\text{Al}_2\text{O}_3/\text{LiCoO}_2$  interface may also contribute to the overall charge transfer.<sup>34,35</sup> Although one superficial semicircle is observed for  $\text{Al}_2\text{O}_3\text{--LiCoO}_2$ , the shape of the semicircle is not symmetric. One semicircle for  $\text{Al}_2\text{O}_3\text{--LiCoO}_2$  includes a small charge-transfer resistance at the  $\text{Al}_2\text{O}_3/\text{LiCoO}_2$  and electrolyte/electrode interfaces. The first semicircle (#) does not change much during cycling. In contrast, the radius of the second semicircle (\*) increases dramatically with the number of charge-discharge cycles. The increases occur both for the real and imaginary impedances, indicating increases in charge-transfer resistance.

For the electrode prepared using  $\text{Al}_2\text{O}_3$  ALD-coated  $\text{LiCoO}_2$  powders, the interface with the electrolyte is very stable. Figure 10 shows that the semicircle for  $\text{Al}_2\text{O}_3$  ALD-coated  $\text{LiCoO}_2$  holds its overall radius and shape even after 50 charge-discharge cycles. There is no indication of increases in charge-transfer resistance. This electrode prepared with  $\text{Al}_2\text{O}_3$  ALD-coated  $\text{LiCoO}_2$  particles is exceptionally stable.

There are several possible mechanisms for the enhancement caused by the  $\text{Al}_2\text{O}_3$  ALD coatings.<sup>6,36</sup> First, the  $\text{Al}_2\text{O}_3$  ALD coating may help suppress the structural instabilities related to lithium in-

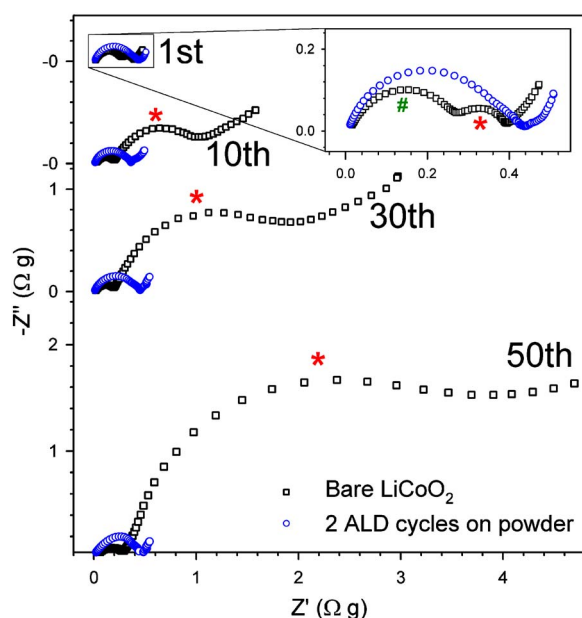


**Figure 10.** (Color online) Series of mass-normalized impedance spectra for electrodes fabricated with bare and  $\text{Al}_2\text{O}_3$  ALD-coated  $\text{LiCoO}_2$  powders for various charge-discharge cycle numbers.

section and desorption.<sup>5,37,38</sup> However, the ultrathin  $\text{Al}_2\text{O}_3$  ALD coating would not have the mechanical strength to withstand lattice expansions, as originally suggested for much thicker  $\text{Al}_2\text{O}_3$  coatings.<sup>5,37,38</sup> Second, the  $\text{Al}_2\text{O}_3$  ALD coating may act as a solid electrolyte and may prevent the direct contact between the cathode surface and the electrolyte.<sup>6,36</sup> The  $\text{Al}_2\text{O}_3$  ALD-covered surface may be less effective for electrolyte decomposition at higher potentials compared with a bare  $\text{LiCoO}_2$  surface. The direct attack of HF that results from the reaction of the trace amounts of water and  $\text{LiPF}_6$  in the electrolyte<sup>39,40</sup> can also be protected by  $\text{Al}_2\text{O}_3$  ALD coating. Consequently, Co dissolution from the  $\text{LiCoO}_2$  particle by the HF attack may be effectively suppressed.<sup>30,41,42</sup> The  $\text{Al}_2\text{O}_3$  ALD film can serve as a scavenger for HF.<sup>43</sup>

XPS was performed on the fabricated electrodes with 4 cycles of  $\text{Al}_2\text{O}_3$  ALD both before and after 10 charge-discharge cycles. Before charge-discharge cycling, the binding energy of the Al 2s peak was 118.7 eV [full width at half-maximum (fwhm) = 2.2 eV]. After 10 charge-discharge cycles, the binding energy of the Al 2s peak was at 119.2 eV (fwhm = 2.8 eV). The Al 2s peak for  $\text{Al}_2\text{O}_3$  could fall in the range of 116.25–119.5 eV, and the Al 2s peak for  $\text{AlF}_3$  could be 121.0 eV.<sup>44</sup> The shift in the binding energy and peak broadening of the Al 2s peak after 10 charge-discharge cycles may indicate the formation of some  $\text{AlF}_3$ .

**ZnO ALD on  $\text{LiCoO}_2$  powders.**—Earlier studies of  $\text{LiCoO}_2$  powders coated with various metal oxides reported that the capacity retention of coated  $\text{LiCoO}_2$  was independent of the specific metal oxide.<sup>45</sup> To determine if the effect of  $\text{Al}_2\text{O}_3$  ALD is unique to  $\text{Al}_2\text{O}_3$ ,  $\text{LiCoO}_2$  powders were also coated using ZnO ALD. ZnO ALD was deposited on  $\text{LiCoO}_2$  powders using four ALD cycles. The stability of the electrodes prepared using the ZnO ALD-coated  $\text{LiCoO}_2$  powders was then compared with electrodes fabricated using the  $\text{Al}_2\text{O}_3$  ALD-coated  $\text{LiCoO}_2$  powders.

Figure 11 shows that the electrodes fabricated with ZnO ALD-coated  $\text{LiCoO}_2$  powders displayed larger overpotentials after 10 and 50 charge-discharge cycles compared with the results for  $\text{Al}_2\text{O}_3$  ALD shown in Fig. 9. Figure 12 also reveals that the ZnO ALD-coated  $\text{LiCoO}_2$  powders displayed a pronounced reduction in capacity with the number of charge-discharge cycles. These results are very similar to the charge-discharge cycle results for bare  $\text{LiCoO}_2$

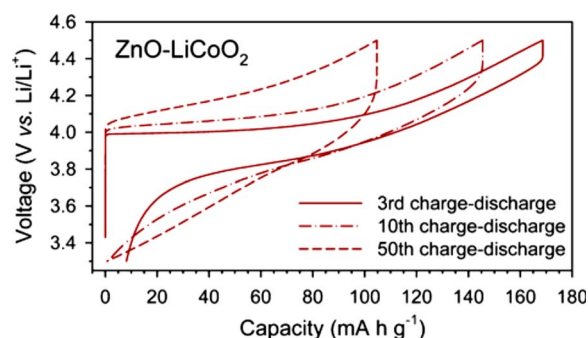


**Figure 11.** (Color online) Charge-discharge voltage profiles of electrodes fabricated using  $\text{Al}_2\text{O}_3$  ALD and ZnO ALD-coated  $\text{LiCoO}_2$  powders at the 3rd, 10th, and 50th charge-discharge cycles.

powders in Fig. 8. In contrast to the results for  $\text{Al}_2\text{O}_3$  ALD, there is no improvement in the cycle performance for the ZnO ALD-coated  $\text{LiCoO}_2$  particles compared with electrodes fabricated with the bare  $\text{LiCoO}_2$  powders.

The ZnO ALD layer may not be stable on the  $\text{LiCoO}_2$  particles. The atomic fraction of  $\text{Zn}[\text{Zn}/(\text{Zn} + \text{Co})]$  and  $\text{Al}[\text{Al}/(\text{Al} + \text{Co})]$  before cycling and after 10 charge-discharge cycles was obtained using XPS. The atomic fraction of Zn dramatically decreased from 0.49 before any charge-discharge cycling to 0.01 after 10 charge-discharge cycles. In contrast, the atomic fraction of Al maintained the same value within experimental error. The initial atomic fraction of Al was 0.55 before cycling and 0.53 after 10 charge-discharge cycles.

These XPS measurements indicate that the  $\text{Al}_2\text{O}_3$  ALD film is more electrochemically stable than the ZnO ALD film. The  $\text{Al}_2\text{O}_3$  ALD film or the resulting  $\text{LiAl}_x\text{Co}_{1-x}\text{O}_2$  solid solution remains on the  $\text{LiCoO}_2$  powders after 10 charge-discharge cycles. In contrast, the ZnO ALD film either diffuses into the  $\text{LiCoO}_2$  powders or dissolves into the electrolyte after 10 charge-discharge cycles. The loss of Zn signal in the XPS spectrum is consistent with no improvement in the performance of the electrodes fabricated using the ZnO ALD-coated  $\text{LiCoO}_2$  powders.

**ALD films on composite electrodes.**—ALD films can also be grown directly on the composite electrode. The internal surfaces of these composite electrodes could be porous and accessible to the ALD precursors. ALD reactants such as TMA diffuse easily into polymers.<sup>46</sup> A similar high diffusion for TMA may be observed in the electrolyte and PVDF polymeric binder. The ALD films cover

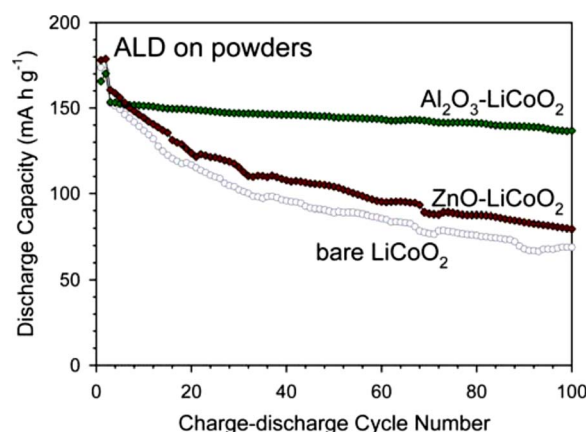


**Figure 12.** (Color online) Cycle performance of electrodes fabricated using bare,  $\text{Al}_2\text{O}_3$  ALD, and ZnO ALD-coated  $\text{LiCoO}_2$  powders. Four ALD cycles were performed on the  $\text{LiCoO}_2$  powders.

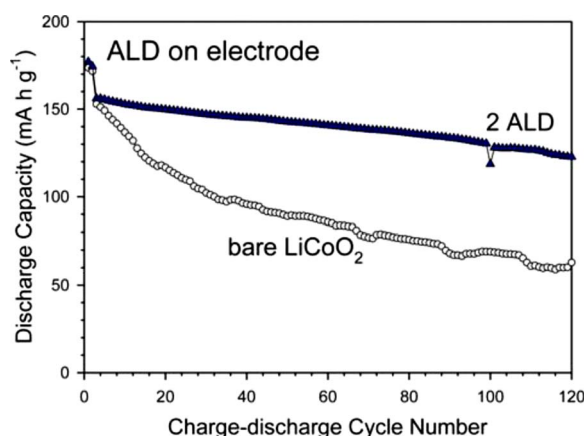


**Figure 13.** (Color online) Charge–discharge cycle performance of bare and  $\text{Al}_2\text{O}_3$  ALD-coated  $\text{LiCoO}_2$  electrodes. Two  $\text{Al}_2\text{O}_3$  ALD cycles were performed on the composite  $\text{LiCoO}_2$  electrode.

any exposed surface of the  $\text{LiCoO}_2$  powders. The only exceptions would be the contact points between the  $\text{LiCoO}_2$  particles and other  $\text{LiCoO}_2$  particles or AB conducting aids.

Figure 13 compares the results for the electrodes prepared using the bare  $\text{LiCoO}_2$  powders and the electrodes prepared using the  $\text{LiCoO}_2$  powders coated with  $\text{Al}_2\text{O}_3$  ALD using two ALD cycles. The capacity retention for  $\text{Al}_2\text{O}_3$  ALD directly on the composite electrodes shown in Fig. 13 is slightly inferior to the capacity retention for ALD on the  $\text{LiCoO}_2$  powders displayed in Fig. 8. However, there is a clear enhancement of capacity vs charge–discharge cycle number compared with the electrodes fabricated using the bare  $\text{LiCoO}_2$  powders. These results confirm the expectation that ALD on the composite electrode has coated the exposed  $\text{LiCoO}_2$  surface area.

**Comparison with previous results.**—Electrodes fabricated using the  $\text{Al}_2\text{O}_3$  ALD-coated  $\text{LiCoO}_2$  powders show a greatly enhanced stability of capacity compared with electrodes fabricated using the bare  $\text{LiCoO}_2$  powders. The enhancement in capacity stability is similar to the improvements observed using much thicker metal oxide coatings deposited using wet chemical methods.<sup>5</sup> However, the  $\text{Al}_2\text{O}_3$  ALD coating of only 3–4 Å can provide the enhancement with a much lower added mass of metal oxide. This lower mass loading would be particularly important to obtain lighter weight Li-ion batteries when using nanoparticle electrodes.

While ZnO coating by chemical methods improves the cycle performance,<sup>47</sup> the ZnO ALD coating does not survive repeated charge–discharge cycling and displays rapid capacity fading. The weight fraction of the coating layer produced by a few ALD cycles is much smaller than the weight fraction produced by chemical methods. The improved cycle performance of ZnO coatings on  $\text{LiCoO}_2$  obtained using chemical methods can be explained by a larger quantity of ZnO that is available to scavenge HF.<sup>43</sup>

ALD may also be a much more efficient method to obtain the metal oxide coatings compared with the solution phase techniques. As a gas-phase method, ALD can deposit the  $\text{Al}_2\text{O}_3$  coating without the use of solvent and with very high reactant efficiency. Reactant efficiencies of nearly 100% can be obtained by using static exposures in rotary ALD reactors<sup>22,23</sup> or by monitoring for a reactant “breakthrough” using a mass spectrometer in fluid bed ALD reactors.<sup>48</sup>

In a previous study, TiN ALD was also used to enhance the interparticle conductivity and cycle rate of the electrodes fabricated using lithium titanate spinel (LTS) particles.<sup>17</sup> An enhanced capacity and cyclability was observed compared with electrodes fabricated using uncoated LTS particles. However, the mechanism for the enhanced performance was unclear. The enhancement could have re-

sulted from an increase in the conductivity between particles. The TiN ALD film could have also formed a passivating layer that protected the LTS particles. Other investigators have observed similar performance to the electrodes fabricated using the TiN ALD-coated LTS particles without any coatings.<sup>49</sup>

**Future prospects.**—ALD shows great potential to enhance the performance of LIBs. Although the results with ultrathin  $\text{Al}_2\text{O}_3$  ALD films are already exceptional, other ALD materials, such as  $\text{TiO}_2$  and  $\text{Ta}_2\text{O}_5$ , may also prove to be useful. ALD can be used to coat the anode and cathode powder materials used to fabricate electrodes. ALD may also be applied directly to the composite electrodes. In contrast, wet chemistry methods are not able to coat the fabricated electrodes. There may be performance or convenience advantages associated with coating either the powders or fabricated electrodes.

ALD is also able to deposit nanolaminates<sup>50</sup> and functionalized films<sup>51</sup> that may serve various purposes. Thin-film nanoengineering is possible using the layer-by-layer control provided by ALD. Molecular layer deposition methods that are similar to ALD and can deposit organic<sup>52,53</sup> or hybrid organic–inorganic<sup>54–56</sup> polymers are also available. These organic and organic–inorganic polymers allow for the tuning of thin-film mechanical properties. This capability may be useful to handle the expansion and contraction during Li insertion and removal.

## Conclusions

Ultrathin  $\text{Al}_2\text{O}_3$  ALD films were grown on  $\text{LiCoO}_2$  powders used as cathodes in LIBs. The ALD coatings dramatically improved the performance of electrodes fabricated with the  $\text{Al}_2\text{O}_3$  ALD-coated  $\text{LiCoO}_2$  powders. The  $\text{Al}_2\text{O}_3$  ALD-coated  $\text{LiCoO}_2$  powders using two ALD cycles showed a capacity retention of 89% after 120 charge–discharge cycles with respect to the reversible capacity at the third charge–discharge cycle. This behavior was observed when cycling in the range of 3.3–4.5 V (vs  $\text{Li}/\text{Li}^+$ ). In contrast, the bare  $\text{LiCoO}_2$  powders maintained only 45% of the initial capacity after the 120 charge–discharge cycles. Similar experiments with ultrathin ZnO ALD films did not display an enhanced performance.  $\text{Al}_2\text{O}_3$  ALD films directly on the composite electrodes fabricated using the bare  $\text{LiCoO}_2$  powders also led to an improvement in performance. The underlying enhancement mechanism may result from the  $\text{Al}_2\text{O}_3$  ALD film minimizing Co dissolution or reducing surface/electrolyte reactions. These promising results for  $\text{Al}_2\text{O}_3$  ALD-coated  $\text{LiCoO}_2$  powders may lead to other opportunities for ALD to improve the performance of LIBs.

## Acknowledgments

This work was funded by a subcontract from a DOE SBIR grant to ALD NanoSolutions (Broomfield, CO). A.S.C. received additional support from the iMINT DARPA Center at the University of Colorado. Y.S.J. also acknowledges a Korea Research Foundation grant (KRF-2008-357-D00066).

University of Colorado assisted in meeting the publication costs of this article.

## References

1. J. M. Tarascon and M. Armand, *Nature (London)*, **414**, 359 (2001).
2. M. S. Whittingham, *Chem. Rev. (Washington, D.C.)*, **104**, 4271 (2004).
3. M. Winter, J. O. Besenhard, M. E. Spahr, and P. Novak, *Adv. Mater.*, **10**, 725 (1998).
4. G. A. Nazri and G. Pistoia, *Lithium Batteries: Science and Technology*, Kluwer Academic, Boston (2004).
5. J. Cho, Y. J. Kim, T. J. Kim, and B. Park, *Angew. Chem., Int. Ed.*, **40**, 3367 (2001).
6. C. Li, H. P. Zhang, L. J. Fu, H. Liu, Y. P. Wu, E. Ram, R. Holze, and H. Q. Wu, *Electrochim. Acta*, **51**, 3872 (2006).
7. J. Cho, Y. W. Kim, B. Kim, J. G. Lee, and B. Park, *Angew. Chem., Int. Ed.*, **42**, 1618 (2003).
8. Y. K. Sun, J. M. Han, S. T. Myung, S. W. Lee, and K. Amine, *Electrochem. Commun.*, **8**, 821 (2006).
9. J. Cho, Y. J. Kim, and B. Park, *Chem. Mater.*, **12**, 3788 (2000).
10. S. M. George, A. W. Ott, and J. W. Klaus, *J. Phys. Chem.*, **100**, 13121 (1996).
11. M. Ritala and M. Leskela, *Atomic Layer Deposition*, Academic, San Diego, CA

- (2001).
12. H. Kim, *J. Vac. Sci. Technol. B*, **21**, 2231 (2003).
  13. M. Knez, K. Niesch, and L. Niinisto, *Adv. Mater.*, **19**, 3425 (2007).
  14. T. M. Mayer, J. W. Elam, S. M. George, P. G. Kotula, and R. S. Goeke, *Appl. Phys. Lett.*, **82**, 2883 (2003).
  15. L. Niinisto, J. Paivasaari, J. Niinisto, M. Putkonen, and M. Nieminen, *Phys. Status Solidi A*, **201**, 1443 (2004).
  16. M. J. Pellin, P. C. Stair, G. Xiong, J. W. Elam, J. Birrell, L. Curtiss, S. M. George, C. Y. Han, L. Iton, H. Kung, et al. *Catal. Lett.*, **102**, 127 (2005).
  17. M. Q. Snyder, S. A. Trebukhova, B. Ravdel, M. C. Wheeler, J. DiCarlo, C. P. Tripp, and W. J. DeSisto, *J. Power Sources*, **165**, 379 (2007).
  18. A. C. Dillon, A. W. Ott, J. D. Way, and S. M. George, *Surf. Sci.*, **322**, 230 (1995).
  19. M. D. Groner, F. H. Fabreguette, J. W. Elam, and S. M. George, *Chem. Mater.*, **16**, 639 (2004).
  20. A. W. Ott, J. W. Klaus, J. M. Johnson, and S. M. George, *Thin Solid Films*, **292**, 135 (1997).
  21. M. D. Groner, J. W. Elam, F. H. Fabreguette, and S. M. George, *Thin Solid Films*, **413**, 186 (2002).
  22. J. A. McCormick, B. L. Cloutier, A. W. Weimer, and S. M. George, *J. Vac. Sci. Technol. A*, **25**, 67 (2007).
  23. J. A. McCormick, K. P. Rice, D. F. Paul, A. W. Weimer, and S. M. George, *Chem. Vap. Deposition*, **13**, 491 (2007).
  24. A. Yamada, B. S. Sang, and M. Konagai, *Appl. Surf. Sci.*, **112**, 216 (1997).
  25. E. B. Yousfi, J. Fouache, and D. Lincot, *Appl. Surf. Sci.*, **153**, 223 (2000).
  26. J. W. Elam and S. M. George, *Chem. Mater.*, **15**, 1020 (2003).
  27. P. J. Cumpson, *Surf. Interface Anal.*, **29**, 403 (2000).
  28. C. J. Powell and A. Jablonski, *NIST Electron-Effective-Absorption-Length Database, NIST SRD 82, Version 1.1*, National Institute of Standards and Technology, Gaithersburg, MD (2003).
  29. L. J. van der Pauw, *Philips Tech. Rev.*, **20**, 220 (1958).
  30. Y. J. Kim, H. Kim, B. Kim, D. Ahn, J. G. Lee, T. J. Kim, D. Son, J. Cho, Y. W. Kim, and B. Park, *Chem. Mater.*, **15**, 1505 (2003).
  31. Y. J. Kim, T. J. Kim, J. W. Shin, B. Park, and J. P. Cho, *J. Electrochem. Soc.*, **149**, A1337 (2002).
  32. S. Oh, J. K. Lee, D. Byun, W. I. Cho, and B. W. Cho, *J. Power Sources*, **132**, 249 (2004).
  33. N. Kosova, E. Devyatkina, A. Slobodyuk, and V. Kaichev, *Solid State Ionics*, **179**, 1745 (2008).
  34. B. Kim, C. Kim, T. G. Kim, D. Ahn, and B. Park, *J. Electrochem. Soc.*, **153**, A1773 (2006).
  35. M. D. Levi, G. Salitra, B. Markovsky, H. Teller, D. Aurbach, U. Heider, and L. Heider, *J. Electrochem. Soc.*, **146**, 1279 (1999).
  36. L. J. Fu, H. Liu, C. Li, Y. P. Wu, E. Rahm, R. Holze, and H. Q. Wu, *Solid State Sci.*, **8**, 113 (2006).
  37. J. Cho, Y. J. Kim, and B. Park, *J. Electrochem. Soc.*, **148**, A1110 (2001).
  38. Z. X. Wang, L. J. Liu, L. Q. Chen, and X. J. Huang, *Solid State Ionics*, **148**, 335 (2002).
  39. D. Aurbach, *J. Electrochem. Soc.*, **136**, 906 (1989).
  40. K. Edstrom, T. Gustafsson, and J. O. Thomas, *Electrochim. Acta*, **50**, 397 (2004).
  41. L. J. Liu, Z. X. Wang, H. Li, L. Q. Chen, and X. J. Huang, *Solid State Ionics*, **152-153**, 341 (2002).
  42. S. Verdier, L. El Ouatani, R. Dedryvere, F. Bonhomme, P. Biensan, and D. Gonbeau, *J. Electrochem. Soc.*, **154**, A1088 (2007).
  43. S. T. Myung, K. Izumi, S. Komaba, Y. K. Sun, H. Yashiro, and N. Kumagai, *Chem. Mater.*, **17**, 3695 (2005).
  44. A. J. Kropf, H. Tostmann, C. S. Johnson, J. T. Vaughey, and M. M. Thackeray, *Electrochem. Commun.*, **3**, 244 (2001).
  45. Z. H. Chen and J. R. Dahn, *Electrochem. Solid-State Lett.*, **6**, A221 (2003).
  46. C. A. Wilson, R. K. Grubbs, and S. M. George, *Chem. Mater.*, **17**, 5625 (2005).
  47. T. Fang, J. G. Duh, and S. R. Sheen, *J. Electrochem. Soc.*, **152**, A1701 (2005).
  48. D. M. King, J. A. Spencer, X. Liang, L. F. Hakim, and A. W. Weimer, *Surf. Coat. Technol.*, **201**, 9163 (2007).
  49. K. Nakahara, R. Nakajima, T. Matsushima, and H. Majima, *J. Power Sources*, **117**, 131 (2003).
  50. F. H. Fabreguette, R. A. Wind, and S. M. George, *Appl. Phys. Lett.*, **88**, 013116 (2006).
  51. C. F. Herrmann, F. H. Fabreguette, D. S. Finch, R. Geiss, and S. M. George, *Appl. Phys. Lett.*, **87**, 123110 (2005).
  52. N. M. Adamczyk, A. A. Dameron, and S. M. George, *Langmuir*, **24**, 2081 (2008).
  53. Y. Du and S. M. George, *J. Phys. Chem. C*, **111**, 8509 (2007).
  54. A. A. Dameron, D. Saghet, B. B. Burton, S. D. Davidson, A. S. Cavanagh, J. A. Bertand, and S. M. George, *Chem. Mater.*, **20**, 3315 (2008).
  55. S. M. George, B. Yoon, and A. A. Dameron, *Acc. Chem. Res.*, **42**, 498 (2009).
  56. B. Yoon, J. L. O'Patchen, D. Seghete, A. S. Cavanagh, and S. M. George, *Chem. Vap. Deposition*, **15**, 112 (2009).